Application of an all-dielectric metamaterial with large spectrum smooth transmission in measuring the jade carving materials

JIANWEI LI[1,2], GE HUANG[1,2,*], QIAN TIAN[3], WEI WU[4], QUANWEI MA[5]
[1]Hezhou University, 542899, Hezhou, China
[2]Key Laboratory of Big Data for Innovative Design in Guangxi Universities, 542899, Hezhou, Guangxi, China
[3]Haikou University of Economics, 570000, Hainan, China
[4]South China Normal University, Shanwei, 516625, Guangdong, China
[5]Jiangxi Institute of Fashion Technology, 330201, Jiangxi, China

An all-dielectric metamaterial is proposed and applied in measurement of the thermal conductivity of jade carving materials. This metamaterial achieves a smooth transmission spectral over a large frequency range, which is different with traditional electromagnetic (EM) metamaterial/metasurface sensors. In the 2-36THz band, the average transmittance and reflectance are: 0.716 and 0.155, and the change in transmittance is relatively small and stable, which is suitable for measuring the transmission spectrum of jade carving samples. The thermal properties of the jade carving sample are weakened with the thickness increasing (from 1mm to 1.6mm), and the sensing sensitivities are: 1.8A/mm, 2.8A/mm, and 2.7A/mm. The heat conduction properties of the four jade carving materials (Jadeite, Turquoise, Color Jade, and Yellow stone) are measured by applying this metamaterial. The measured thermal diffusion coefficients are: 3.41, 2.72 , 4.65, and 3.75. And the measured thermal resistance coefficients are:15.38, 12.32, 20.79, and 16.64. This metamaterial is suitable for measuring the thermal conduction properties of jade carving materials.

1. Introduction

Electromagnetic metamaterials are artificially designed and prepared materials with periodic micro/nanostructures, and many novel resonant behaviors are achieved, such as: negative refraction and perfect absorption [1-3]. These reported resonance properties are excited by the interference and coupling between incident electromagnetic waves and metal resonators. Therefore, obvious resonance absorption, transmission or reflection peaks are achieved by these reported EM metamaterials/metasurfaces [4-10]. Based on the resonance absorption and transmission characteristics, the EM metamaterials/metasurfaces have been applied to develop a variety of sensors [11-14]. By measuring the difference between these absorption peaks or transmission peaks (amplitude or resonant frequency), environmental changes can be detected to achieve sensing purposes [11-14]. At present, metamaterial-based sensors have been applied in many fields, such as: temperature sensing, liquid sensing, current sensing, etc [15-20].

However, these reported sensors are not suitable for measuring jade carving materials, paper materials, clothing materials, etc. This is because these reported sensors all excite significant resonance modes (absorption mode or transmission mode) in the operating frequency band [11-20]. On the contrary, these materials (jade carving materials, paper materials, clothing materials) all have significant large frequency range smooth performance spectral lines (transmission spectral lines, or absorption spectral lines). These distinct resonance modes will cover a part of the characteristic spectral lines of these materials [11-20]. The measurement errors and the complexity of signal processing will be increased. Therefore, to measure the transmission spectrum of jade carving samples, corresponding metamaterial sensors also need to have similar large frequency range transmission spectrum characteristics.

Here, a metamaterial with wide frequency range and smooth transmission spectral characteristics is developed in 2-36THz. This metamaterial adopts an all-dielectric structure strategy (without metal layers). The measured average transmittance and reflectance are 0.716 and 0.155 in the operating frequency range of 2-36THz. Therefore, the spectral characteristics of this metamaterial sensor is suitable for measuring the thermal conduction performance of jade carving samples, which is different with these reported sensors [11-20]. The influence of structural parameters on the transmission performance is measured. When the thickness of the jade carving samples is increased,

the thermal conductivity properties (the thermal response current is reduced, the thermal diffusion coefficient is reduced, and the thermal resistance is increased) are weakened. In addition, due to the different composition, the type of jade carving also directly affects the thermal conductivity performance.

2. Structure and samples

In order to achieve stable transmission performance, the recommended metamaterial is an all-dielectric material that does not contain any metal layers: MgF2, SU-8, and Si, as shown in Fig. 1. The top layer of MgF2 adopts a circular hole array, and the middle layer SU-8 and bottom layer Si are both intact. All geometric parameters are shown in Table 1. All simulation results are obtained using simulation software HFSS. In the simulation process, the boundary conditions of the structural cells are used with ideal electrical guides and ideal magnetic guides. The electromagnetic force is coming from directly above the structure. In the simulation process, the grid cells and dimensions are automatically matched by the simulation system without manual settings. A perfectly matched layer is applied to the bottom of the structural unit to eliminate scattering losses. The scanning step of the frequency is 0.002THz. The preparation of the metamaterial sample can be carried out using the following steps: (a) A silicon nitride layer is set to be a temporary substrate. This temporary substrate is fixed in the center of a glue spinner and a 1mm thick SU-8 layer is covered on this temporary substrate. The using device: MSC-400Bz-6 N spinner, spin speed is 1850

rpm, spin time is 6 min. Then, this SU-8 layer is heated and cured by using a hot plate. The using device: C-MAG HP10, the heated temperature is 96 0C, for 8 min. (b) This temporary substrate is fixed in the center of the vacuum coating machine and a Si layer is covered on the SU-8 layer. The using device: ZZL-U400C, vacuuming time is 5 h, warm-up time is 38 min, at a rate 2.1 Ås^{-1}, working pressure is $55e^{-10}$ (atm). (c) After the Si layer cooled, the temporary substrate is fixed in the center of the glue spinner and a 5 μm thick SU-8 layer is covered on the Si layer. Then this new SU-8 layer is also heated and cured by using the same hot plate (C-MAG HP10, the parameters are the same). (d) After the SU-8 layer cooled, the temporary substrate is fixed in the center of the same vacuum coating machine and a MgF2 layer is covered on the new SU-8 layer. The using device: ZZL-U400C, vacuuming time is 5 h, warm-up time is 32 min, at a rate 1.9 Ås^{-1}, working pressure is $55e^{-10}$ (atm). (e) The proposed circular hole array on the MgF2 layer is achieved by the etching machine (CABL-9000C), as shown in Fig. 1(c), (f) The measured transmittance, thermal response current, thermal diffusion coefficient, and thermal resistance are achieved by the Bruker Optics Equinox. The sample is fixed using a double-sided clamp. The excitation port of electromagnetic wave is 10 cm away from the sample, and the receiving port is 8 cm away from the sample. Normal temperature and pressure. The measuring chamber is sealed. (g) The proposed metamaterial sample is cleaned by ultrasonic wave. And the photo of the metamaterial sample was obtained using Leica DM2700, as shown in Fig. 1 (c).
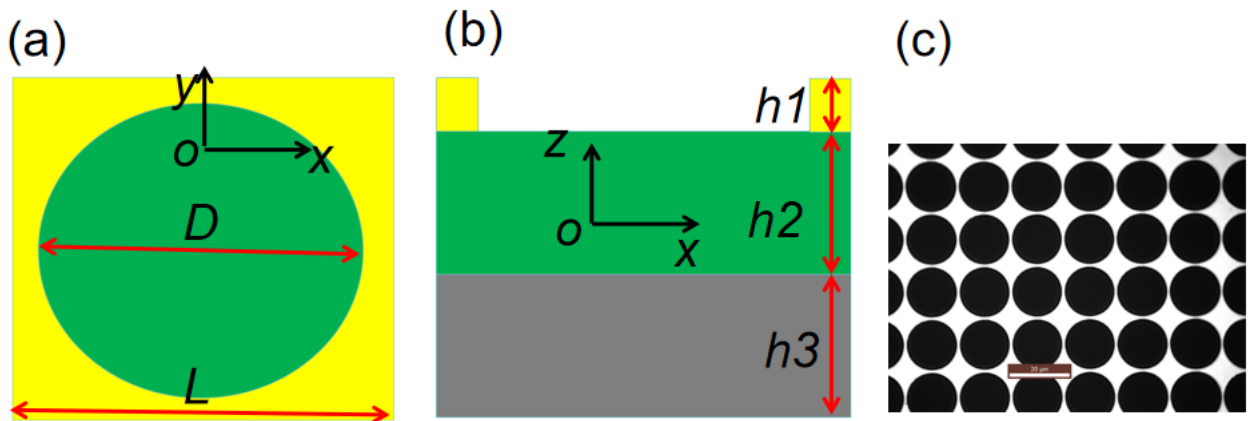

Fig. 1. (a) Top view of the proposed metamaterial. (b) Side view of the proposed metamaterial structure. (c) Optical photos of the suggested metamaterial samples. In this metamaterial structure, the yellow part is the MgF2 layer, the green part is the SU-8 layer, and the gray part is the Si layer (colour online)

Table 1. Geometric parameters

Parameter	L	D	h_1	h_2	h_3
Value(μm)	20	19	0.5	5	2

3. Results and discussion

3.1. Transmission mechanism of metamaterial samples

The metamaterial sample is measured under normal temperature and pressure conditions, with the electromagnetic wave emission port and reflection receiving port located 10cm above the sample. The electromagnetic wave is vertically incident on the surface of the sample, and the transmittance receiving port is located 8cm directly below the sample. This first set of measurements is to verify the transmission performance of the metamaterial, and the measurement results are shown in Fig. 2. In the target frequency range of 2-36THz, the average transmission value of the metamaterial sample is about 0.716, and the fluctuation amplitude of transmission is about 0.03, as shown by the black curve in Fig. 2. Meanwhile, the average values of reflectance and absorption are 0.155 and 0.129, respectively. In 2-36THz, the fluctuation amplitudes of reflectivity and absorption are about 0.02 and 0.04, as shown by the red and blue spectral lines in Figure 2. These measurement results indicate that the metamaterial sample exhibits performance characteristics of wide frequency range and stable transmittance within the target frequency range of 2-36THz, which is different with these sensors [11-20]. The proposed metamaterial sample has the potential to be used for measuring the thermal conductivity of jade carving samples. At the same time, in order to verify the electromagnetic resonance properties of the metamaterial, the equivalent medium theory is applied [21]. The equivalent permittivity and equivalent permeability of the proposed metamaterial structure are calculated as follows:

$$\varepsilon_{eff}(\lambda) = \varepsilon_o \cdot (\varepsilon_\infty - \frac{c_o^2/\lambda_e^2}{c_o^2/\lambda^2 - jc_o\gamma_e/\lambda}) \qquad (1)$$

$$\mu_{eff}(\lambda) = \mu_o \cdot (1 - \sum_{i=1}^{2} \frac{F_i c_o^2/\gamma_e^2}{c_o^2/\lambda - c_o^2/\lambda_{mi}^2 - jc_o\gamma_{mi}/\lambda_{mi}}) \qquad (2)$$

Here, the ε_{eff} is the effective permittivity, and the μ_{eff} is the effective permeability. The other parameters are: the F_i is the filling factor. The C_0 is the speed of light in free space. The is the γ damping factor. According to the formulae (1-2), the equivalent refractive index and the equivalent impedance can be expressed as:

$$z_{eff}(\lambda) = \sqrt{\frac{\mu_{eff}}{\varepsilon_{eff}}} \qquad (3)$$

$$n_{eff}(\lambda) = \sqrt{\mu_{eff}} * \sqrt{\varepsilon_{eff}} \qquad (4)$$

The equivalent refractive index and equivalent impedance of the metamaterial structure are obtained and shown in Fig. 2 (b-c). In the operating band 2-36THz, the average value of the real part of the equivalent impedance is 0.835, and the average value of the real part of the equivalent refractive index is -1.02, as shown in Fig. 2 (b-c). Since the real part of the equivalent impedance is close to 1, the energy loss of the electromagnetic wave during penetration of the metamaterial structure is suppressed. At the same time, the average real part of the equivalent refractive index is -1.02, resulting in the reflection loss of electromagnetic wave is also weakened. These electromagnetic resonance properties excite the high transmission properties of the metamaterial sample, as shown in Fig. 2 (a). It should be pointed out that in the operating band 2-36THz, the maximum difference of the equivalent impedance is about 0.004, and the maximum difference of the equivalent refractive index is about 0.007, as shown in Fig. 2 (b-c). This proposed metamaterial structure has stable electromagnetic resonance characteristics in this frequency band. Therefore, the obtained transmission performance is also stable in the operating band 2-36THz, as shown in Fig. 2 (a). These calculated electromagnetic characteristics meet the measurement requirements of the thermal conductivity of jade carved samples.
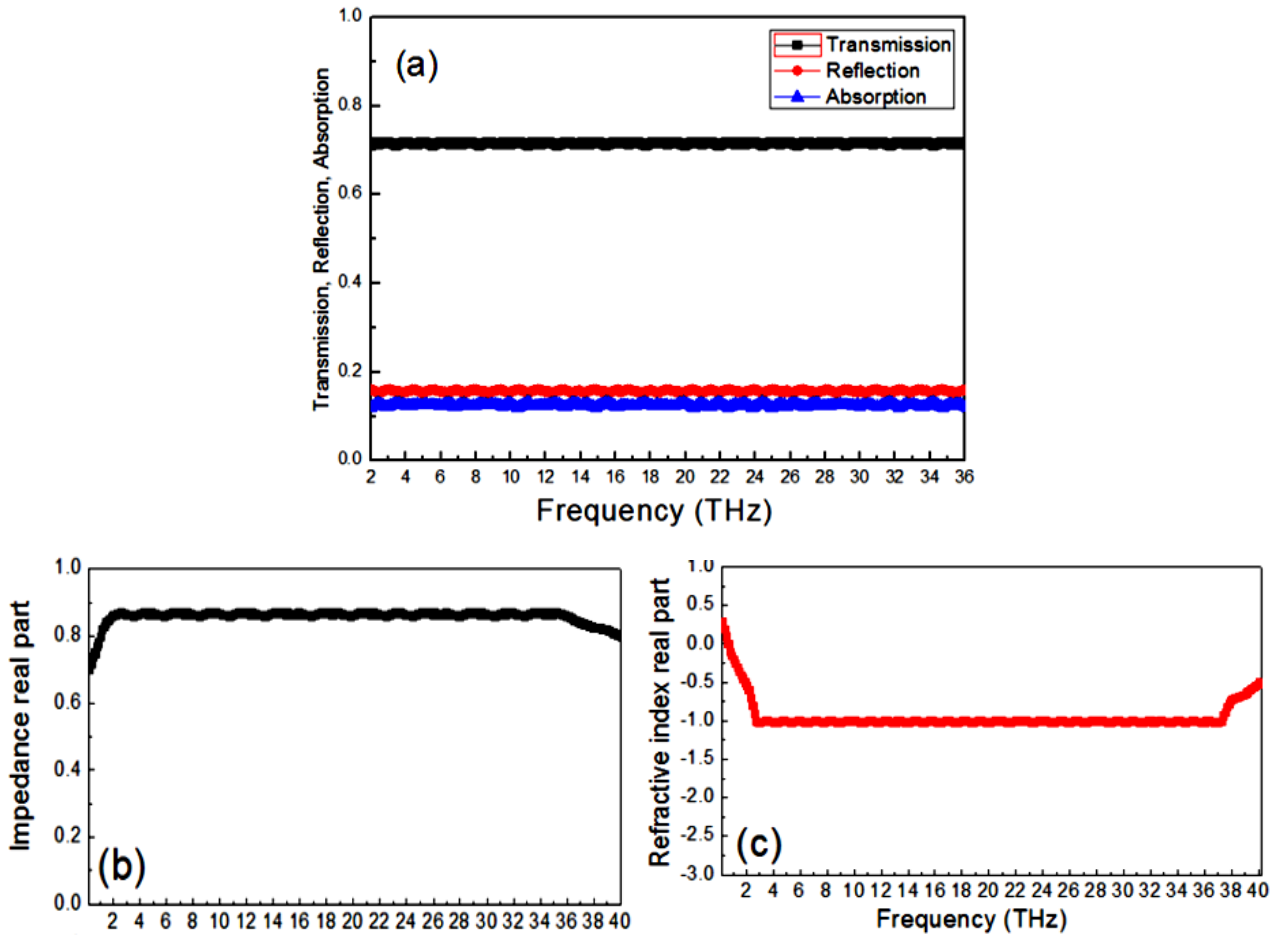
Fig. 2. (a) Measurement results of the transmission, reflection, and absorption properties of the proposed metamaterial. (b) The real part of the equivalent impedance. (c) The real part of the equivalent refractive index (colour online)

In order to understand the transmission characteristics of the metamaterial, the electric field intensity distributions during the process of electromagnetic waves penetrating the structural unit are simulated and shown in Fig. 3. In the target frequency range of 2-36THz, the electric field strengths at two frequency points are obtained, as shown in Fig. 3 (b-c). When the calculated frequency point is 6THz, the energy of the electromagnetic wave is uniformly distributed inside the dielectric layers SU-8 and Si during the penetration of the sample, and is dispersed in the bottom air layer, as shown in Fig. 3 (b). At frequency points 6THz and 32THz, when the electromagnetic wave penetrates the metamaterial sample, no resonance modes (such as absorption mode or transmission mode) are excited, as shown in Fig. 3 (b-c) (the electric field intensity inside the dielectric layers SU-8 and Si is basically uniform).

Out of 2-36THz, two frequency points are also simulated, at 0.5THz, and 40THz, as shown in Fig. 3 (a, d). At the frequency point 0.5THz, the electromagnetic wave is coupled with the circular hole array of the metamaterial structure and excites the corresponding resonant absorption mode during the penetration of the sample, as shown in Fig 3(a). Most energy of the electromagnetic wave is absorbed by the coupled electric field, as shown in Fig 3(a). At the frequency point 40THz, Similar energy absorption phenomena can also be observed. These energy absorption modes do not meet the sensing requirements of smooth spectrum in large frequency range. This indicates that the metamaterial absorber can effectively achieve stable transmission performance in the frequency range of 2-36THz.
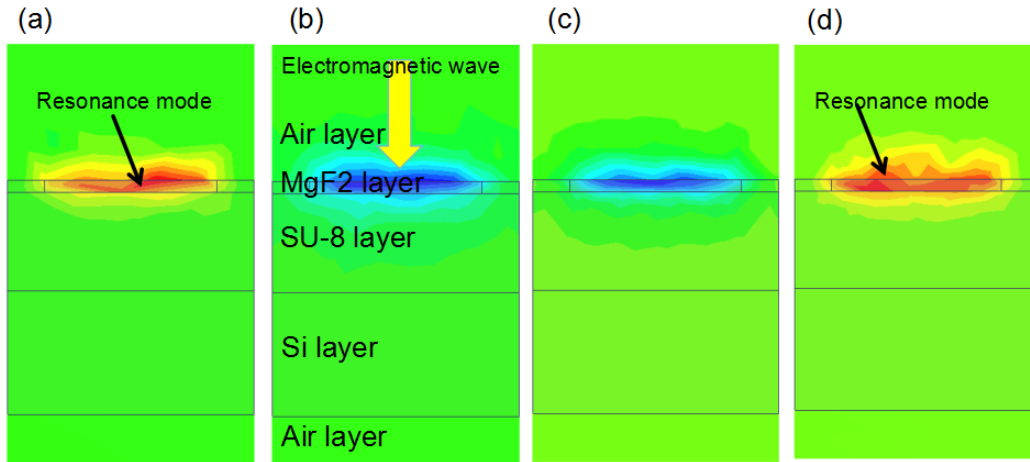
Fig. 3. Simulation results of electric field intensity distributions. The closer the color is to red, the stronger the electric field is. (a) 0.5THz. Outside the operating frequency band, a distinct resonance mode is excited, which does not meet the sensing requirements. (b) 6THz. In the operating frequency band, no significant resonance mode is excited, which meets the sensing requirements. (c) 32THz. In the operating frequency band, no significant resonance mode is excited, which meets the sensing requirements. (d) 40THz. Outside the operating frequency band, a distinct resonance mode is excited, which does not meet the sensing requirements (colour online)

3.2. The relationship between the transmission performance of metamaterials and structural parameters

According to the simulation results in Fig. 3, it can be seen that the transmission performance of the metamaterial is related to the dielectric layers SU-8 and Si. In order to intuitively understand the influence of the dielectric layers SU-8 and Si on the transmission spectrum, the structural parameter $h2$ is gradually increased in the second set of experiments, as shown in Fig. 4(a). The structural parameters $h2$ is set to be: 5 μm, 6 μm, and 7 μm, respectively. The average transmittance values of the metamaterial sample are: 0.716, 0.682, and 0.664, respectively, as shown in Fig. 4. During the gradual thickening of the dielectric layer SU-8, the transmission spectrum of the metamaterial sample is basically stable, and the transmission fluctuation amplitudes during three measurement processes are: 0.03, 0.04, and 0.03, respectively. The total thickness difference in experiments is 2 μm, while the total transmittance difference is only 0.052, as shown in Fig. 4(a). This is because of the dielectric layer SU-8 is a high transmittance and low loss material in the terahertz band. The SU-8 layer has no resonance absorption characteristic for electromagnetic waves in the terahertz frequency band. Therefore, as the thickness of SU-8 increases, the transmittance of the metamaterial is slightly and steadily reduced. In the third experiment, the structural parameter $h3$ is gradually increased, as shown in Fig. 4(b). When the structural parameter $h3$ is increased to 3 μm, the average transmittance of the metamaterial sample is reduced to 0.598, as shown by the red curve in Fig. 4(b). When the structural parameter $h3$ is continuously increased to 4 μm, the average transmittance of the metamaterial sample is reduced to 0.501, as shown by the blue curve in

Fig. 4(b). In the third set of experimental measurements, the transmission fluctuation amplitudes of the metamaterial sample are: 0.003, 0.002, and 0.002, respectively. This stability is similar to the measurement results in Fig. 4(a). In Fig. 4 (b), the thickness difference of the dielectric layer Si is still 2 μm (consistent with Fig. 4 (a)), but the total transmittance difference of the metamaterial sample reached 0.215, as shown in Fig. 4(b). This is because the dielectric layer Si has a higher loss of electromagnetic wave energy than the SU-8. When the thickness of Si layer is increased, the overall transmission property of the metamaterial sample is weakened, as shown in Fig. 4 (b). It should be noted that the Si layer also has no resonance absorption mode for electromagnetic waves in the terahertz frequency band. Therefore, the transmission spectrum obtained in the experiment is still smooth. The thickness of the dielectric layers Si and SU-8 is related to the transmission amplitude of the metamaterial sample, but does not affect the stability of the measurement results.

The effects of other structural parameters on the transmission properties of the metamaterial are also measured, as shown in Fig. 5. When the thickness of MgF2 layer at the top is gradually increased ($h1$=0.5 μm, 0.6 μm, and 0.7 μm), the average transmittance of the metamaterial is: 0.716, 0.710, and 0.704, as shown in Fig. 5 (a). When the lattice constant of the metamaterial is gradually increased (L=20 μm, 22 μm, and 24 μm), the transmission property of the metamaterial is weakened, and the average measured transmittance is: 0.716, 0.687, and 0.642, respectively, as shown in Fig. 5 (b). When the diameter of the circular hole array is gradually reduced (D=19 μm, 17 μm, and 15 μm), the transmission performance was significantly inhibited, with the average values of 0.716, 0.658, and 0.603, as shown in Fig. 5 (c).

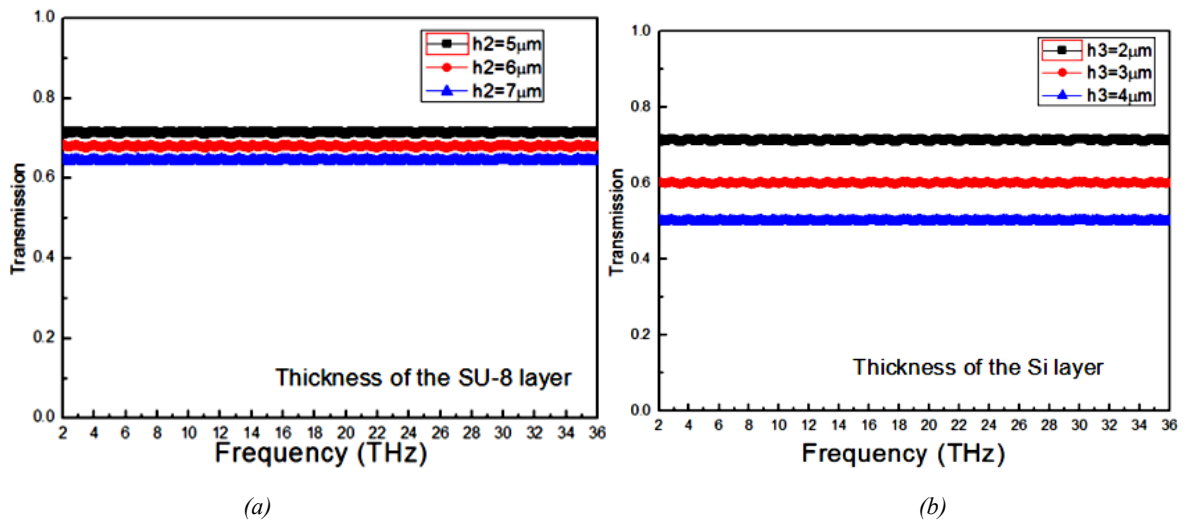*(a)*   *(b)*

Fig. 4. (a) Measurement results of the transmission performance of the metamaterial sample under different structural parameters h2 (Thickness of the SU-8 layer). (b) Measurement results of the transmission performance of the metamaterial sample under different structural parameters h3 (Thickness of the Si layer) (colour online)
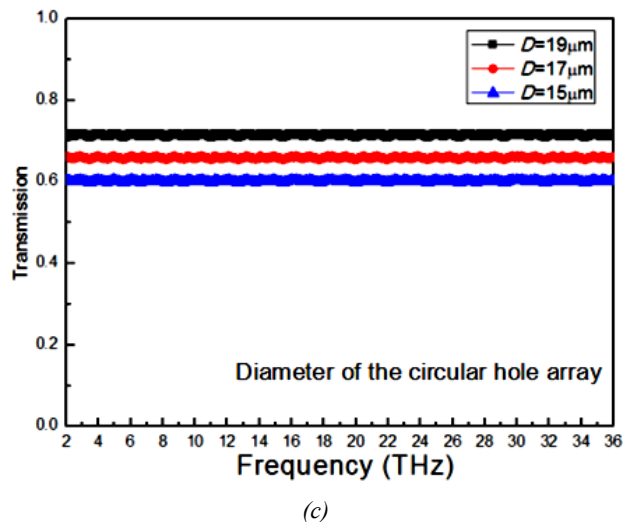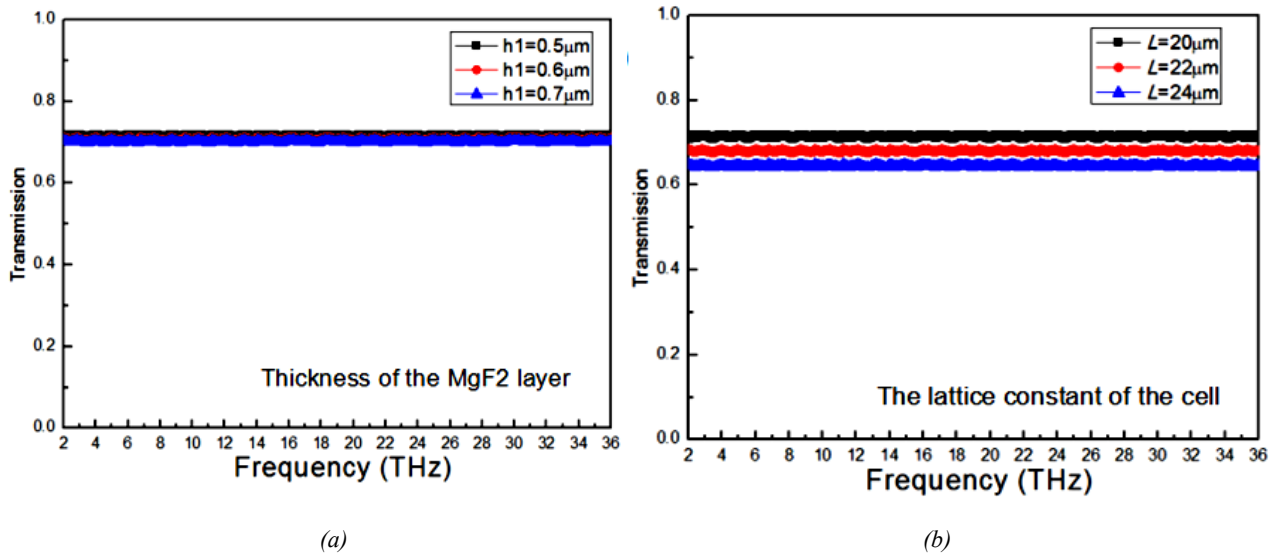

(a)   *(b)*

(c)

Fig. 5. (a) Measurement results of the transmission performance of the metamaterial sample under different structural parameters h1 (Thickness of the MgF2 layer). (b) Measurement results of the transmission performance of the metamaterial sample under different structural parameters L (The lattice constant of the cell). (c) Measurement results of the transmission performance of the metamaterial sample under different structural parameters D. (The diameter of the circular hole array) (colour online)

The MgF2 layer at the top is a typical material with high transmission and low loss. The thickness h1 is increased by 0.2 μm, and the energy lost by electromagnetic wave in penetrating the MgF2 layer is very little, only 0.012, as shown in Fig. 5 (a). On the contrary, when the structural parameter L is increased or D is decreased, the effective area of the circular hole array at the top layer is directly reduced, resulting in more energy being reflected into the air and weakening of the transmission performance, as shown in Fig. 5 (b-c).

3.3. Applying this metamaterial sample to measure the thermal conductivity of jade carving materials

The transmission measurement results shown in Figs. 2, 4, and 5 confirm the characteristic of the metamaterial sample with a large frequency band stationary transmission spectrum. In the fourth experiment, the metamaterial sample is applied to measure the thermal conductivity of jade carving samples (with a type of Jadeite and a thickness of 1mm under normal temperature and pressure conditions). During the measurement process, the metamaterial sensor is located above the jade carving sample Jadeite, as shown in Fig. 6 (b). The energy carried by electromagnetic waves is transferred from the metamaterial above to the jade carving material below, as shown in Fig. 6 (b). In the process of energy conduction and diffusion inside the jade carving material, it will stimulate the weak deformation of the jade carving material, thus forming a thermal response current. Fig. 6(a, c) shows the measurement results of transmittance and reflectance of the Metamaterial + Jade carving samples. Within the operating frequency range of 2-36THz, the average amplitude of transmittance is 0.524 and the average amplitude of reflectance is 0.248. More importantly, the fluctuation amplitude of transmittance is only 0.08, and the reflection fluctuation amplitude is only 0.05, as shown in Fig. 6(a). During the measurement process, the trend of the thermal response current of the jade carving sample Jadeite over time is obtained, as shown in Fig. 6 (c). The thermal diffusivity and thermal resistance of the jade carving material can be obtained by extracting these thermal response currents through the amplifying circuit. It should be noted that the thermal response current is gradually strengthened over time. The amplitude of the thermal response current is slowly increased between 0.00s and 1.75s.

This is because the jade carving sample has thermal conductivity (thermal resistance and thermal diffusion phenomena coexist). The energy carried by electromagnetic waves is suppressed by thermal resistance during the diffusion process inside the jade carving sample. On the contrary, from 1.75s to 2.93s, the amplitude of the thermal response current is sharply increased, as shown in Fig. 6 (c). More and more energy is diffused into the interior of the jade carving sample Jadeite through the transmission of electromagnetic waves. The amplitude of the thermal response current is enhanced by this energy. When the measurement time exceeds 2.93s, the amplitude of the thermal response current tends to stabilize, with an average amplitude of about 7.34, as shown in Fig. 6 (c). This is because the conducted energy has become saturated. When the measurement time exceeds 2.93 seconds, the conduction speed of the energy carried by the electromagnetic wave inside the jade carving sample tends to be stable and uniform.

In order to gain a deeper understanding of the thermal conductivity of the jade carving sample (Jadeite), the thermal resistance and thermal diffusion coefficient are synchronously measured in the experiment and shown in Fig. 7. In the working frequency range of 2-36THz, the average thermal diffusion coefficient of the jade carving sample is about 3.41, and the fluctuation amplitude of the diffusion coefficient is about 0.02, as shown in Fig. 7 (a). This indicates that the thermal diffusion coefficient in this experiment (under normal temperature and pressure conditions, the thickness of the jade carving sample has not been changed) is basically stable and predictable. The measurement results of thermal resistance are revealed in Fig. 7 (b). The average amplitude of thermal resistance is 15.38, with a fluctuation amplitude of approximately 0.01, as shown in Fig. 7 (b). The thermal resistance exhibits stability similar to the thermal diffusion coefficient during the measurement process. By comparing the results of Fig. 6 and Fig. 7, it can be seen that the thermal conductivity (thermal diffusion coefficient and thermal resistance) of this jade carving material is basically stable in the range of 2-36THz. Therefore, when the energy is conducted inside the jade carved sample and reaches a saturated state, a stable thermal response current can be excited. The measurement results in Fig. 7 indicate that it is feasible to use the metamaterial sensor to measure the thermal conductivity of the jade carving sample.

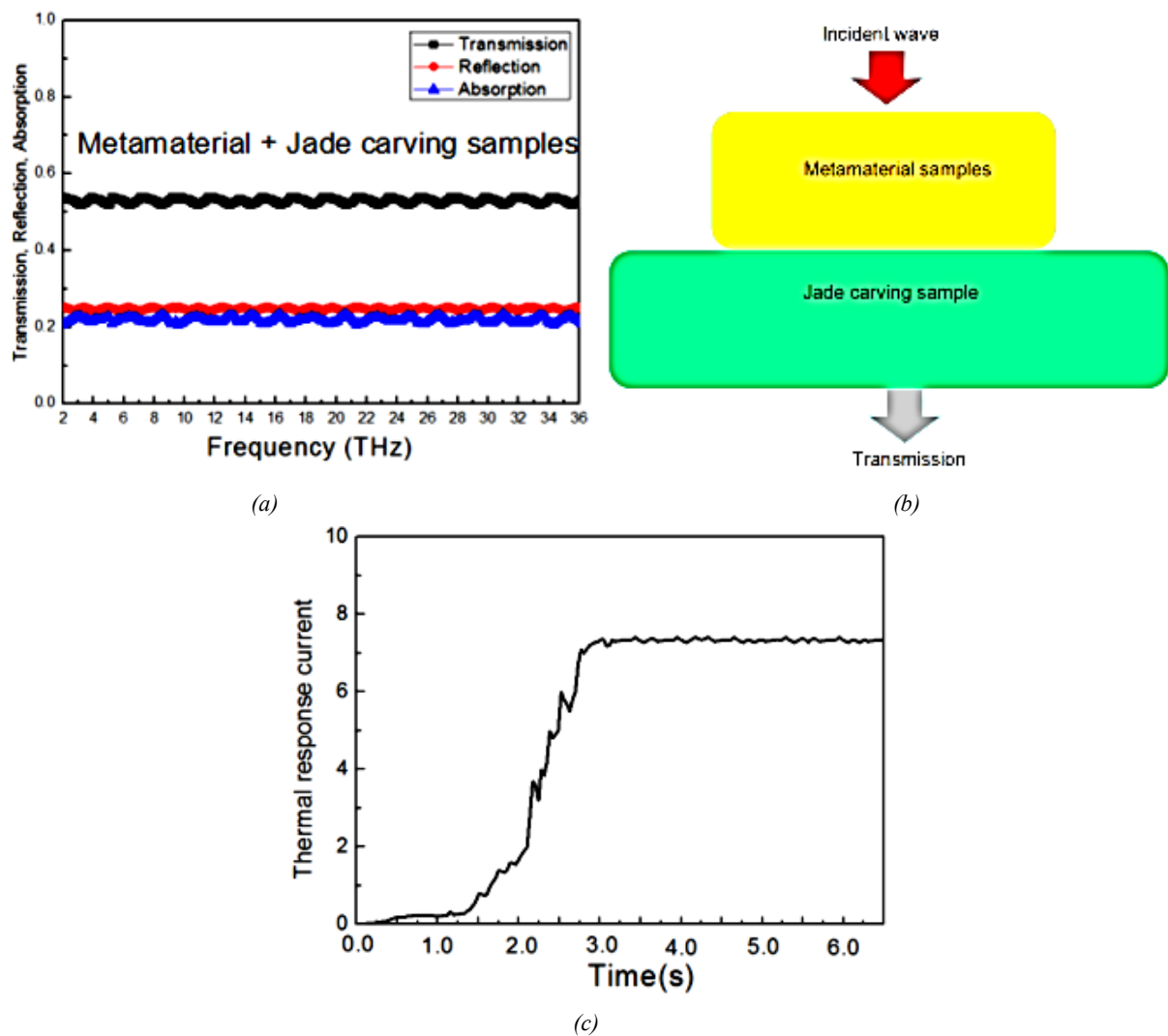*(a)*   *(b)*

(c)

Fig. 6. (a) Measurement results of transmittance, reflectance, and absorption of the Metamaterial + Jade carving samples. (b) Measurement schematic diagram of composite structure of Metamaterial + Jade carving samples. (c) Thermal response current measurement results of the Jade carving samples. The thickness of the Jade carving samples (Jadeite) is 1mm (colour online)

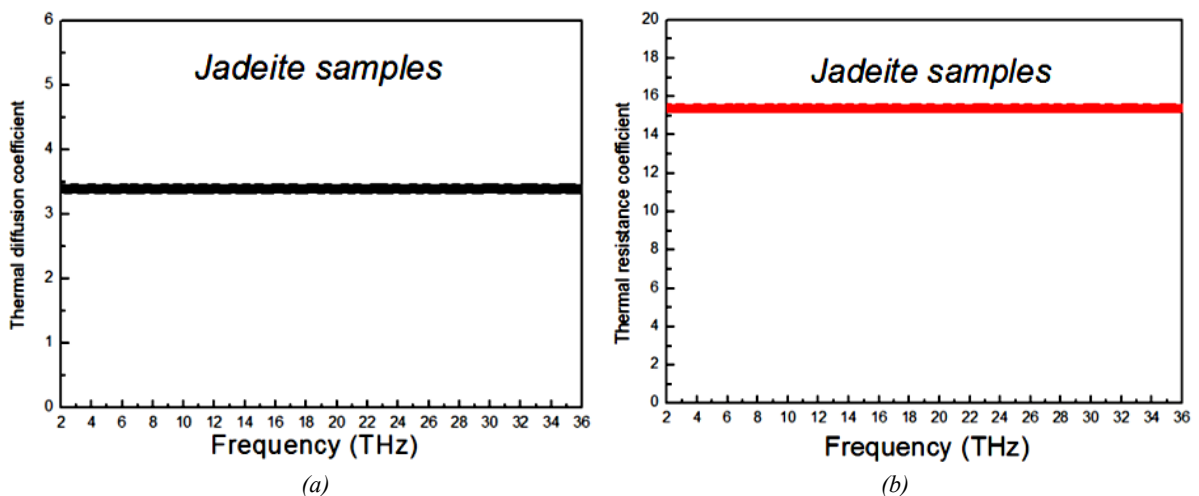*(a)*   *(b)*

Fig. 7. (a) Measurement results of thermal diffusion coefficient of jade carving samples (Jadeite). (b) Thermal resistance measurement results of jade carving samples (Jadeite). The thickness of the Jade carving samples (Jadeite) is 1mm under normal temperature and pressure conditions (colour online)

In the fifth experiment, the effect of thickness on thermal conductivity is revealed, as shown in Fig. 8. The thickness of the jade carving sample Jadeite is set to be: 1mm, 1.2mm, 1.4mm, and 1.6mm, respectively. When the thickness is increased to 1.2mm, the time required for the thermal response current to increase from the minimum to the maximum is about 3.32 seconds, as shown by the red curve in Fig. 8. When the thickness is continuously increased, the time required for the thermal response current to reach its maximum value is 3.62 seconds and 4.11 seconds, respectively, as shown by the green and blue curves in Fig. 8. The stable values of the measured thermal response currents are: 7.34, 6.98, 6.42, and 5.88, as shown in Fig. 8. Due to the use of the same type of jade carving samples, the resonance trend of thermal response current is similar under different thickness conditions. The measurement results in Fig. 8 show that the metamaterial is sensitive to the thickness of the jade carving sample. The sensitivity of the metamaterial in the process of measuring the thermal corresponding current of the jade carving sample is expressed as:

$$S_i = \left| \frac{\Delta i}{\Delta h} \right| \tag{5}$$

In the above formula, S_i is the sensitivity of the thermal response current, Δh is the thickness difference of the jade carving sample, Δi is the difference of the thermal corresponding current obtained from two adjacent measurements. The heat reaching the surface of the jade specimen will excite the corresponding thermal response current. A DC amplifier circuit (36V for DC voltage) is used to extract these thermal response currents and obtain the corresponding thermal diffusion coefficient and thermal resistance synchronously, as shown in Fig. 6 (c). The extracted thermal response current, thermal diffusivity and thermal resistance are displayed via an oscilloscope. It should be pointed out that as the thickness increases, the amplitude of the thermal response current gradually decreases, and the time required to reach the amplitude gradually increases. Therefore, by measuring the amplitude

of the thermal response current, the thickness change of the jade carving sample can be revealed. According to formula (5), the cubic sensing sensitivity obtained during the thickness increase process is: 1.8A/mm, 2.8A/mm, and 2.7A/mm. According to these sensing results, it can be seen that in the two adjacent measurement processes, the amplitude difference of the thermal response current of the jade carving sample becomes larger and larger, which leads to the sensing sensitivity of the metamaterial becoming larger and larger (according to formula (5)).

These measurement sensitivities reveal the relationship between the thickness of the carved jade sample and the thermal response current. At the same time, these measurements also show that the diffusion rate of energy inside the jade carving sample is gradually decreasing. Therefore, the thermal conductivity of the jade carving sample is weakened with increasing thickness. The extracted thermal response current, thermal diffusivity and thermal resistance are revealed:

$$P_{Xuan-paper} = P_{All-structures} - P_{Ambient} \tag{6}$$

$$I(t) = \frac{A}{d} \int_o^d g(y) \frac{\partial \Delta \theta(y,t)}{\partial t} dy \tag{7}$$

$$g(y) = (a_\varepsilon - a_y)\varepsilon_o \varepsilon_r E(y) + P_{Xuan-paper}(y) \tag{8}$$

$$R_{Substrate} = \frac{h_3}{k_{Substrate}} \tag{9}$$

$$R_{Xuan-paper} = \frac{h_2}{k_{Xuan-paper}} \tag{10}$$

$$R_{sensor} = \frac{h_1}{k_{sensor}} \tag{11}$$

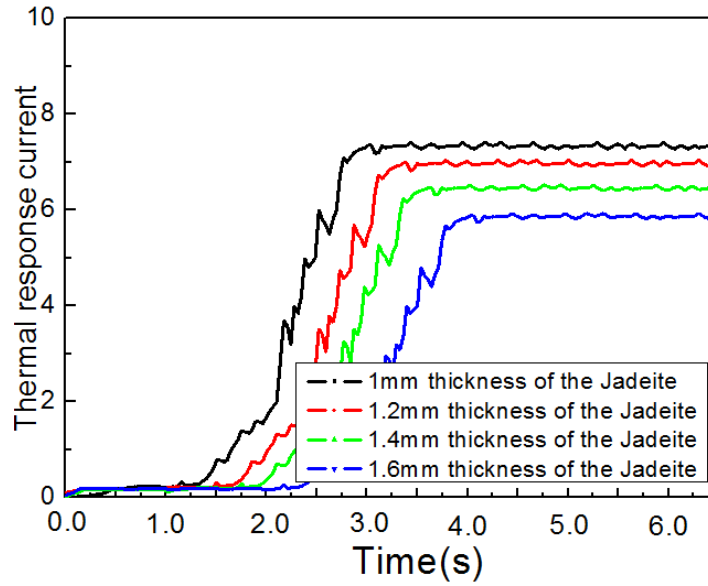$$R_{Overall} = R_{sensor} + R_{Xuan-paper} + R_{Substrate} \tag{12}$$

Fig. 8. Measurement results of thermal response current under different thickness conditions. During the measurement process, the thickness of the jade carving sample Jadeite is set to: 1mm, 1.2mm, 1.4mm, and 1.6mm, respectively. The thickness of the metamaterial sensor remains constant during measurement at normal temperature and pressure (colour online)

The thermal diffusion coefficient and thermal resistance of jade carving samples under different thickness conditions are measured, as shown in Fig. 9. The measurement results of thermal diffusion coefficients are: 3.41, 3.23, 2.72, and 2.03, as shown in Fig. 9 (a). Within the operating frequency range (2-36THz), the fluctuation amplitude of the thermal diffusion coefficients is: 0.02, 0.01, 0.02, and 0.02, respectively. During the measurement process, the total difference in thickness of 0.6mm resulted in a decrease of 1.38 in the thermal diffusion coefficient. Obviously, the thickness of the jade carving sample has a significant impact on the diffusion of energy. Meanwhile, the measurement results of thermal resistance are: 15.38, 16.47, 18.05, and 21.09, as shown in Fig. 9 (b). Similarly, the thermal resistance is also basically stable within 2-36THz. According to similar sensing calculation principles, the thermal diffusion coefficient and thermal resistance sensitivities of the jade carved sample are:

$$S_d = \left| \frac{\Delta diffusion}{\Delta h} \right| \qquad (13)$$

$$S_r = \left| \frac{\Delta resistance}{\Delta h} \right| \qquad (14)$$

According to formula (13), the measured sensitivities of the thermal diffusion coefficient are：0.9m^2/s*mm, 2.55m^2/s*mm, and 3.45m^2/s*mm. At the same time, the

measured sensitivity of the thermal resistance is:5.45m^{2}K/W*mm, 7.9m^{2}K/W*mm, and 15.2m^{2}K/W*mm (Based on formula (14)). Comparing these sensitivity measurements, it can be seen that the metamaterial is sensitive to changes in the thermal response current of the jade carving sample Jadeite. It should be pointed out that as the thickness of the jade carving sample Jadeite is gradually increased, the sensing sensitivity of the metamaterial is also gradually increased. These measurements indicate that the thickness of the jade specimen is an important factor in determining the heat conductivity. Therefore, by changing the thickness, the thermal conductivity of the jade carving sample Jadeite can be modulated. It should be pointed out that the application of metamaterial-based devices to the sensing field is one of the research hotspots. Many metamaterial sensors have been proposed, optimized and measured, such as refractive index sensors, biosensors, medical sensors, etc. [22-27]. These proven metamaterial sensors can excite single or multiple absorption/transmission peaks in the operating frequency range. When the ambient medium is changed, the resonant properties of these reported sensors (resonance frequency, amplitude) are controlled. Changes in the environmental medium can be detected by measuring the difference in resonance properties and calculating the corresponding sensing sensitivity, as shown in Table 2. However, unlike these proven sensors, the proposed metamaterial does not effectively excite single or multiple absorption peaks in the operating frequency band, as shown in Fig. 2. The

transmission spectrum, absorption spectrum and reflection spectrum are smooth curves in the operating frequency band, as shown in Fig. 2. Thus, the proposed metamaterial can be used for sensing purposes by measuring the difference in amplitude of the transmission spectrum, as shown in Figs. 8 and 9. In addition, metamaterial sensors have been applied in many fields, such as temperature sensing, voltage/current sensing, refractive index sensing, biosensing, and medical sensing [15-20, 22-27]. However, metamaterials have not been applied to the thermal conductivity sensing of jade carving materials. The measurement results in Figs. 8 and 9 verify the feasibility of this proposed metamaterial for thermal conductivity sensing, which is different from the reported metamaterial sensors [15-20, 22-27]. The heat conduction properties of jade carving materials Jadeite are stable and smooth in a large spectrum range, as shown in Figs. 7, 8 and 9. These reported metamaterial sensors all have obvious resonance absorption peaks and are not suitable for measuring the heat conduction properties of jade carving materials [15-20, 22-27].

Finally, in the sixth experiment, the relationship between the type of jade carving sample and its thermal conductivity was measured. Four types of jade carving samples are: Jadeite, Turquoise, Color Jade, and Yellow stone. During the measurement process, the thickness of these jade carving samples is 1mm, at room temperature and pressure, using the same metamaterial sensor and the same wave source and receiving device. The thermal response current amplitude of the jade carving sample Turquoise is 5.73, and the required time is 3.47 seconds, as shown by the red curve in Fig. 10. The thermal response current amplitude of the jade carving sample Color Jade is 9.33, and

the required time is 2.03 seconds, as shown by the green curve in Fig. 10. The thermal response current amplitude of the jade carving sample Yellow stone is 7.92, and the required time is 2.64 seconds, as shown by the blue curve in Fig. 10. Among the four jade carving samples, Turquoise samples took the most time to reach the peak thermal response current. In addition, the amplitude of the thermal response current is minimal. On the contrary, the response current of Color Jade sample takes the least time to reach the peak value, while the amplitude of the thermal response current is the largest. The thermal response current of different jade carving samples shows significant differences, including amplitude and required time. These phenomena are related to the substances contained in different types of jade carving samples. The physical characteristics of the jade carving samples (including the main composition, density, hardness, dielectric constant, permeability etc.) are important factors that lead to the difference of the thermal response current measurement results.

According to the results in Fig 10, it can be seen that under the same measurement conditions, the type of jade carving material is the key factor determining the heat conduction performance. Simultaneously, the thermal diffusivity and thermal resistance of these jade carving materials are also measured, as shown in Fig. 11. In Fig. 10, the amplitude of the thermal response current of the Jade carving sample Turquoise is the lowest, which means that the diffusion coefficient of energy inside this sample is also weakened. In the target frequency range of 2-36THz, the average thermal diffusion coefficient of jade carving sample Turquoise is 2.72, which is the lowest among the four samples, as shown in the red curve in Fig. 11 (a).

Table 2. Results of the proposed metamaterial compared with reported metamaterial sensors.

|	*Operating spectrum*	*Resonance characteristic*	*Sensing type*
[22]	0.2-0.7THz	Single transmission peak	Biosensing
[23]	108-120THz	Single transmission valley	Biosensing
[24]	1-9THz	Six absorption peaks	Medical sensing
[25]	0.1-0.35THz	Single transmission valley	Refractive index sensing
[26]	4.0-6.0THz	Four absorption peaks	Refractive index sensing
[27]	30-90 μm	Single absorption peak	Refractive index sensing
This work	2-36THz	Single transmission band	Thermal conduction sensing
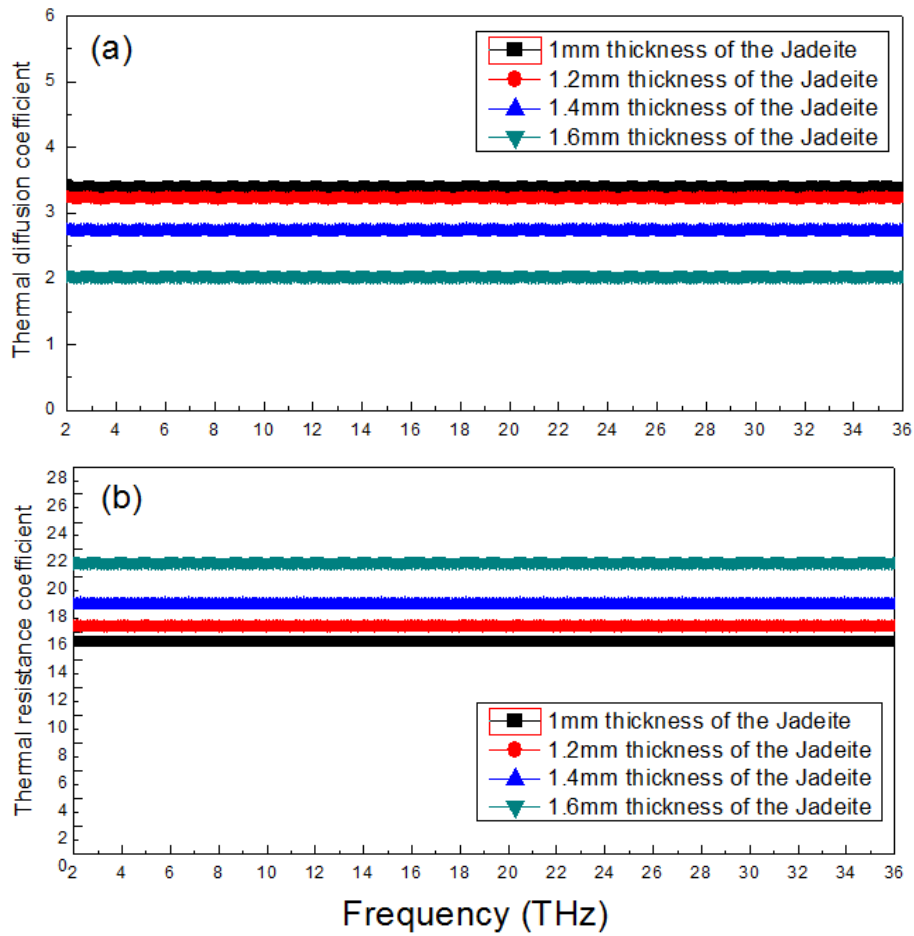
Fig. 9. During the measurement process, the thickness of the jade carving sample Jadeite is set to be: 1mm, 1.2mm, 1.4mm, and 1.6mm, respectively. (a) Measurement results of thermal diffusion coefficient under different thickness conditions. (b) Measurement results of thermal resistance coefficient under different thickness conditions. The thickness of the metamaterial sensor remains constant during measurement at normal temperature and pressure (colour online)
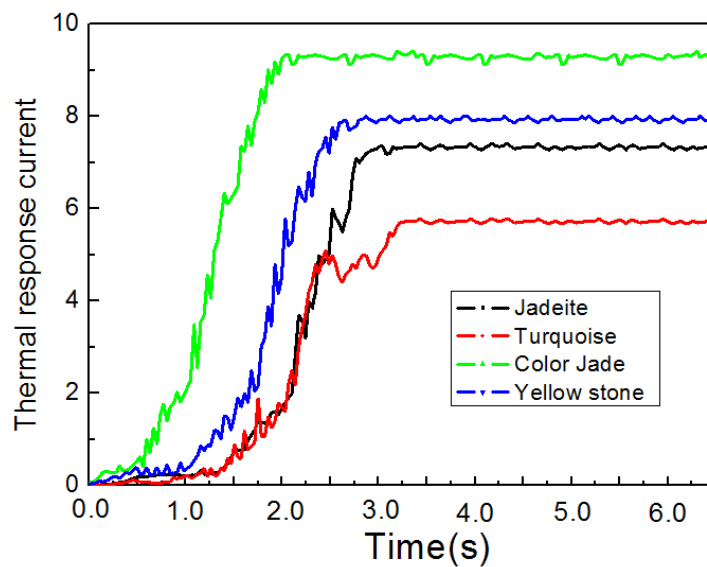

Fig. 10. Measurement results of thermal response current for different jade carving samples (Jadeite samples, Turquoise samples, Color Jade samples, Yellow stone samples). All of the thickness of the four jade carving samples is 1mm (colour online)
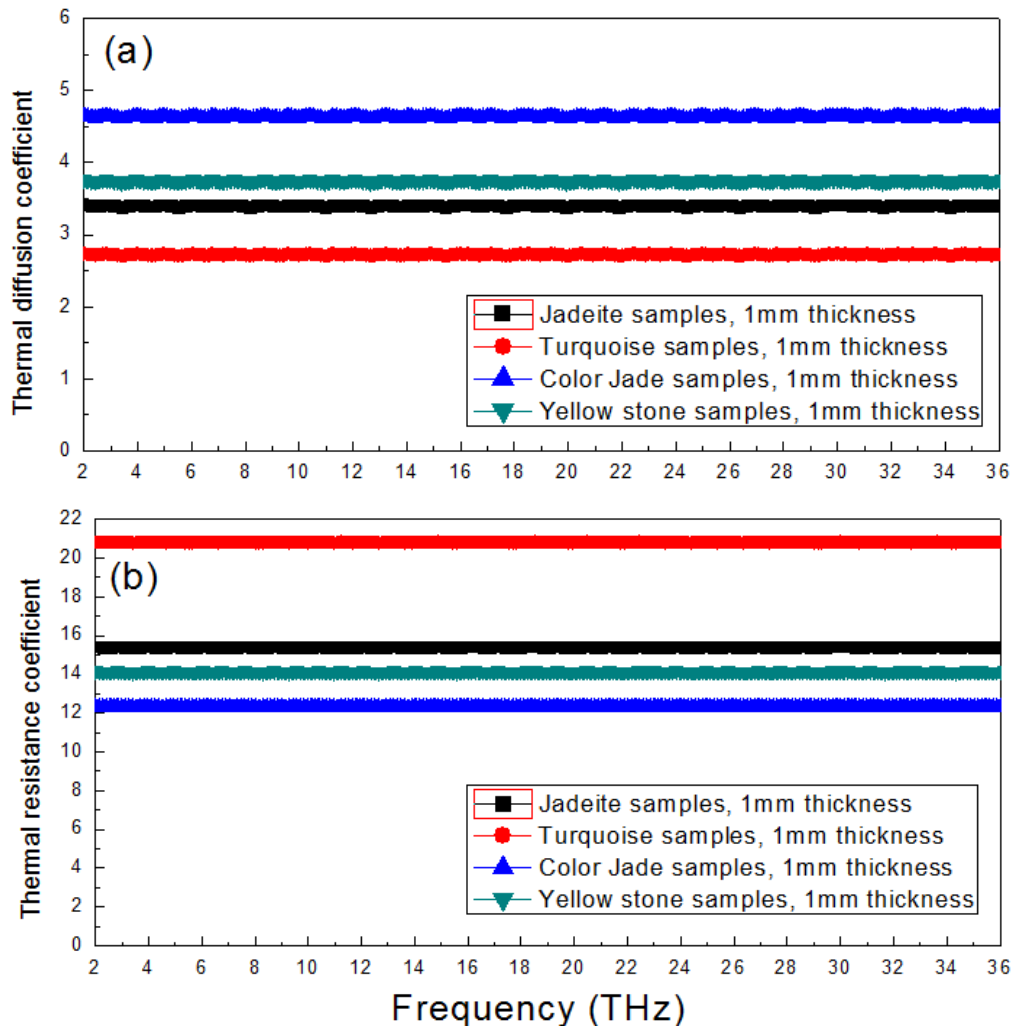
Fig. 11. (a) Measurement results of thermal diffusion coefficients for different jade carving samples. (b) Thermal resistance measurement results of different jade carving samples. All of samples are 1mm thickness. The measuring condition is normal temperature and pressure (colour online)

The corresponding average thermal resistance is 20.78, the highest of the four measurements, as shown by the red curve in Fig. 11 (b). These measurements indicate that Turquoise has the lowest thermal conductivity among the four samples, as shown in Fig. 11. In contrast, the Jade carving sample Color Jade has the highest mean thermal diffusion coefficient (4.65) and the lowest mean thermal resistance (12.32). Therefore, the heat conduction capacity of the Jade carved sample Color Jade is the highest among the four samples. In addition, The average thermal diffusion coefficient and thermal resistance of the Jade carving sample Yellow stone are 3.75 and 16.64, respectively. The heat conduction capacity of the jade carved Yellow stone is close to that of the Jadeite samples, as shown in Fig. 11.

The difference between the heat conduction properties of these jade carving samples is mainly based on the significant difference in the composition. Due to the significant differences in the minerals contained, the diffusion rate of energy within the sample is limited to varying degrees. These measured jade carving samples all have stable thermal conductivity (in the target frequency range of 2-36THz). The measurement results in Figs. 8, 9, 10, and 11 indicate that the proposed metamaterial sensor can be effectively used to measure the thermal conductivity of jade carving samples.

4. Conclusion

In the operating frequency range of 2-36THz, this proposed metamaterial achieves an average transmittance of 0.716 and an average reflectance of 0.155. Moreover, the change in transmittance is relatively small and stable in the process of optimizing structural parameters. The measured thermal response current, diffusion coefficient, and resistance of the Jadeite carving sample are: 7.34, 3.41, and 15.38. Moreover, the thermal conductivity properties of the Jadeite carving sample is weakened with increasing thickness (from 1mm to 1.6mm). Finally, the thermal conductivity (thermal response current, thermal diffusion coefficient, and thermal resistance) of different kinds of Jade carving materials (Jadeite, Turquoise, Color Jade, and Yellow stone) is measured by applying this metamaterial. The proposed metamaterial can be applications for measuring jade carving materials.

Declaration of interests

The authors declare that they have no known competing financial interests or personal relationships that could have appeared to influence the work reported in this paper.

Acknowledgments

References

[1] M. Nejat, N. Nozhat, Sensors **19**(22), 10490 (2019).

[2] M. Y. Azab, M. F. O. Hameed, A. M. Nasr, S. S. Obayya, Sensors **21**(6), 7748 (2021).

[3] M. R. Nickpay, A. Shahzadi, M. Danaie, Superlattices and Microstructures **150**, 106786 (2021).

[4] D. Subramaniyam, P. M. Bruntha, C. Priya, International Journal of Engineering **33**(11), 2215 (2020).

[5] F. Lotf, N. Sang-Nourpour, R. Kheradmand, Optics and Laser Technology **137**, 106809 (2021).

[6] P. M. Bruntha, D. Subramaniyam, B. K. Pandey, T. M. Neebha, D. Pandey, K. M. Sagayam, Aerospace Systems **6**(1), 53 (2022).

[7] F. O. Alkurta, O. Altintasa, M. Ozakturk, M. Karaaslana, O. Akgola, E. Unala, C. Sabahc, Physics Letters A **384**, 126041 (2020).

[8] J. Huang, Y. Yi, G. Niu, Z. Yi, Z. Zhou, X. Chen, X. Ye, Y. Yi, Y. Tang, T. Duan, Physica Scripta **94**(8), 085805 (2019).

[9] M. Omri, F. Ouerghi, F. Abdelmalek, S. Haxha, Sensors **20**(15), 8505 (2020).

[10] J. T. Wen Liu, W. P. Rongcao Yang, Current Applications in Physics **31**, 122 (2021).

[11] H. Hu, X. Huang, Y. Zhao, X. Zhang, Y. Wang, B. Qi, Frontiers in Physics **10**, 990126 (2022).

[12] T. M. Neebha, A. D. Andrushia, S. P. Dhanasekar, A. Varshney, R. Manjith, Journal of Electromagnetic Waves and Applications **37**(6), 814 (2023).

[13] A. S. Saadeldin, M. F. O. Hameed, E. M. A. Elkaramany, S. S. A. Obayya, Sensors **19**(18), 7993 (2019).

[14] F. Qin, Y. Yi, T. Duan, X. Chen, W. Yao, Z. Yi, P. Wu, G. Li, H. Yang, Z. Chen, Nanomaterials **10**(2), 207 (2020).

[15] Z. Song, K. Wang, J. Li, Q. H. Liu, Optics Express **26**, 7148 (2018).

[16] Y. I. Abdulkarim, L.W. Deng, M. Karaaslan, E. Unal, Chemical Physics Letters **732**, 136655 (2019).

[17] H. J. Zou, Y. Z. Cheng, Optical Materials **88**, 674 (2019).

[18] Qiu Wang, Eric Plum, Quanlong Yang, Xueqian Zhang, Quan Xu, Yuehong Xu, Jiaguang Han, Weili Zhang, Light: Science and Applications **7**, 25 (2018).

[19] Tong Cai, Hai-Peng Li, Lei Zhou, Scientific Reports **6**, 27503 (2016).

[20] Z. C. Guo, K. H. Wen, Q. Y. Hu, W. H. Lai, J. Y. Lin, Y. H. Fang, Sensors **18**, 1348 (2018).

[21] K. E. Oughstun, S. Shen, Journal of the Optical Society of America B **5**, 2395 (1988).

[22] Gangqi Wang, Fengjie Zhu, Tingting Lang, Jianjun Liu, Zhi Hong, Jianyuan Qin, Nanoscale Research Letters **16**, 109 (2021).

[23] Fariba Lotfi, Nafiseh Sang-Nourpour, Reza Kheradmand, Plasmonics **17**, 799 (2022).

[24] Prince Jain, Himanshu Chhabra, Urvashi Chauhan, Krishna Prakash, Akash Gupta, Mohamed S. Soliman, Md. Shabiul Islam, Mohammad Tariqul Islam, Scientific Reports **13**, 1792 (2023).

[25] Pengyu Liu, Zihao Liang, Zhicheng Lin, Zefeng Xu, Ruijia Xu, Dongyuan Yao, Yu-sheng Lin, Scientific Reports **9**, 9917 (2019).

[26] Jinjun Bai, Wei Shen,Shasha Wang, Meilan Ge,
     Tingting Chen, Pengyan Shen, Shengjiang Chang,
     Optical and Quantum Electronics **53**, 506 (2021).

[27] S. Dhanasekar, K. Martin Sagayam,
     Binay Kumar Pandey, Digvijay Pandey,
     Plasmonics **19**, 2273 (2024).

[*]Corresponding author email: huangge8712@163.com